RSC Advances

PAPER

View Article Online
View Journal | View Issue

Cite this: *RSC Adv.*, 2026, **16**, 15420

Insights into tautomerism and pH effects on the photoluminescence of citric acid-derived molecular fluorophores

Laura Estévez * and Nicolás Otero

Understanding the photoluminescent (PL) behavior of citric acid (CA)-derived carbon dots (CACDs) requires accounting for the contribution of molecular fluorophores (MFs) formed *in situ* during synthesis. Among these, citrazinic acid (CZA), CAGly – derived from CA and glycine, and 4-hydroxy-1*H*-pyrrolo[3,4-*c*]pyridine-1,3,6(2*H*,5*H*)-trione (HPPT) exhibit donor–acceptor groups capable of tautomerization and protonation–deprotonation equilibria, making their PL properties highly sensitive to pH and solvent effects. In this work, we combine CREST screening with DFT/TD-DFT calculations to explore the tautomeric landscape of neutral and ionized forms of these MFs in both ground (S_0) and excited (S_1) states. Our results reveal that the keto tautomer (DPR moiety) predominates in S_0 for CZA and CAGly, whereas the enol tautomer (recovering the 2-pyridone ring) becomes the main phototautomer in S_1 through an excited-state intramolecular proton transfer (ESIPT) process, accurately reproducing previously reported experimental emission wavelengths. This mechanism is strongly influenced by pH and is facilitated by water molecules that lower the ESIPT barrier, revealing the effect of solvent. For HPPT, PL arises from competing pathways involving ESIPT and excited-state deprotonation (ESDP), accounting for a large Stokes shift and pH-independent emission up to pH 10. Overall, these findings evidence that excitation-dependent fluorescence in CACDs may be better explained by tautomeric equilibria and proton-transfer dynamics rather than anti-Kasha behavior, providing a molecular-level framework for tuning optical properties in carbon-based luminescent materials.

Received 8th January 2026
Accepted 12th March 2026

DOI: 10.1039/d6ra00206d

rsc.li/rsc-advances

Introduction

Carbon dots (CDs)[1] have garnered significant attention within the research community due to their outstanding properties, including high fluorescent quantum yields (QYs), facile synthesis, excellent stability, good biocompatibility and low toxicity.[2–4] These characteristics make CDs highly promising for diverse applications such as bioimaging, light-emitting diodes (LED), energy conversion and storage, and photocatalysis.[5–7] CDs produced *via* bottom-up approaches commonly employ citric acid (CA) as the carbon source combined with a nitrogen-containing precursor. Citric acid-derived CDs (CACDs) are particularly attractive because they often exhibit strong fluorescence, rely on inexpensive starting materials, and benefit from the wide availability of nitrogen sources. These nitrogen-containing compounds act as dopants during CACD synthesis, with α, β- and α,γ-diamines, β- and γ-aminoalcohols, β- and γ-aminothiols, urea, and formamide, being the most effective ones for enhancing photoluminescence (PL) emission intensity.[8,9]

The understanding of the reactions occurring during thermal treatment of CA with different nitrogen sources has improved markedly, though the correlation of photoluminescence of CACDs with their structure still lacks a comprehensive model. In particular, the core–shell model does not always fit with the experimental results.[10] The mechanism of the molecular photoluminescence of CACDs has gained much attention recently, and several studies describing the formation of small fluorophore species at reaction conditions applied in CD synthesis are particularly noteworthy.[11,12] Thus, a significant number of research works indicate the high importance of PL-emitting low-molecular weight compounds formed at an incipient stage or concurrently with the formation of CDs, as they significantly contribute to photoluminescence properties of CACDs.[13,14] Indeed, great effort has been made to identify the structure of these molecular fluorophores (MFs) and nowadays the structures of many of these MFs are well-documented.[8,11–15]

Typically, these MFs contain donor and acceptor groups capable of intramolecular proton transfer, including keto–enol tautomerization, which may imply the coexistence of tautomers in dynamic equilibrium. Since structural changes between tautomeric forms are accompanied by variations in physicochemical properties,[16–18] identifying the dominant tautomer – or

Universidade de Vigo, Departamento de Química Física, Facultade de Química, Vigo, 36310, Spain. E-mail: lestevez@uvigo.es

a set of them – is essential for understanding their optical behaviour.[19,20] The presence of these functional groups in the molecular structure suggests that the surrounding pH will govern the equilibrium between neutral and ionized species, potentially resulting in distinct photoluminescent (PL) properties.[21] Thus, CACDs and MFs have been explored as pH sensing probes.[21–24] Furthermore, it has been shown that tautomerism and aggregation could cooperate in shaping the PL output and that under extreme pH, protonation or deprotonation-driven aggregation further generated new, weakly emissive species.[25–27] Aggregation into H- or J-type assemblies is known to generate new excitonic states and red- or blue-shifted emission, as reported for citrazinic-acid-based systems and other carbon-derived fluorophores. Moreover, pH-dependent protonation/deprotonation can promote or suppress such aggregation, thereby influencing the balance between emissive pathways. While aggregation is not the focus of the present study, these effects are acknowledged here as they may conceptually coexist with tautomerism in related systems. Therefore, characterization of the dominant tautomeric and ionized forms will afford critical guidance for evaluating the aggregation structures most likely to occur.

The blue-emitting citrazinic acid (CZA) is the most studied compound of this class obtained as the product of thermal condensation of CA and ammonia in 1893 by Sell and Easterfield.[28] Later,[15] it was found that upon heating of mixtures of urea and citric or citrazinic acid under anhydrous conditions, a green-emitting fluorophore can be readily obtained, identified as (4-hydroxy-1*H*-pyrrolo[3,4-*c*]pyridine-1,3,6(2*H*,5*H*)-trione – HPPT), featuring as well proton donor and acceptor groups leading to possible coexistence of tautomers.[29] This investigation[15] also found that depending on the conditions, allowing water evaporation or not, HPPT or CZA, respectively, can be obtained exclusively.

Scheme 1 outlines a stepwise mechanism for the formation of CZA and HPPT, guided by the mechanistic considerations discussed in ref. 15. Notably, the reaction between CA and NH_3 proceeds analogously to the pathway proposed for MFs derived from CA and amino acids, including glycine (CAGly).[8] According to this mechanistic scheme, the structure obtained for CZA differs from the commonly depicted representation. Instead, it resembles a dioxo-pyridine-ring (DPR)-containing MF, like CAGly,[8] but optical properties of CZA have never been associated with those exhibited by DPR-type MFs.[8] The structure most frequently used to represent CZA corresponds to what we labelled as the enol tautomer (featuring the 2-pyridone moiety), rather than the keto tautomer (comprising the DPR ring).

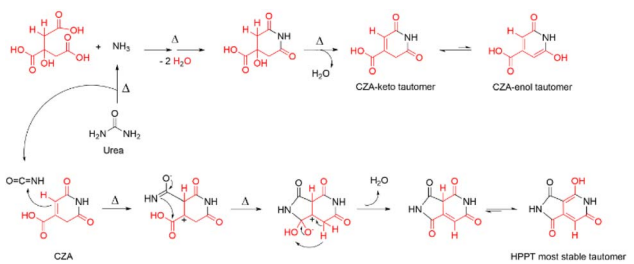

Scheme 1 Stepwise formation of CZA and HPPT. In red, atoms belong to CA; in black, atoms belong to urea.

Compared to CA-based MFs containing the 2-pyridone ring, which typically exhibit high PL QY and well-defined emission governed by Kasha's rule, DPR-type fluorophores display markedly different photophysical behaviour: lower QY and excitation dependent fluorescence, often explained by invoking anti-Kasha's emission.[8,30] However, this phenomenon may also be attributed to emitters undergoing tautomerization, each with a S_1 emitting state, or explained by the coexistence of multiple tautomers in the S_0 ground state, each characterized by distinct excitation and emission wavelengths.[18,31] Several studies[32–36] have shown that many molecular systems and nanomaterials exhibit dual emission and large Stokes shifts arising from Excited-State Intramolecular Proton Transfer (ESIPT). These studies demonstrate that proton donors/acceptors and hydrogen-bond networks strongly modulate the efficiency of ESIPT and the associated activation barriers.

In this work, we demonstrate that the most stable tautomer of CZA in the S_0 state is the keto form (Scheme 1). However, this is no longer the case in the S_1 state, where an ESIPT process leads to the formation of the CZA enol phototautomer. We also investigate the effect of pH on the tautomers.

We expand the study to two other MF's: HPPT and CAGly, the latter serving as a representative DPR-type MF. While its structural characterization was reported in 2017 (ref. 8) and has not been further expanded upon, this experimental assignment remains the only available reference and has not been challenged in subsequent research.

Our results demonstrate that the coexistence of several tautomers of neutral and their ionized counterparts, each with unique photoluminescent (PL) properties, highlights the complexity of the system and its sensitivity to the environment, providing a plausible alternative explanation for the excitation-dependent emission that does not require invoking anti-Kasha behavior.[37,38]

We use computational chemistry methods as they offer a reliable means to achieve these objectives, particularly in cases where experimental techniques may lack sensitivity—especially for detecting multiple tautomers arising from rapid intramolecular proton transfer processes[39,40]—or, as demonstrated below, when the tautomer responsible for emission only appears in the excited state.

Results and discussion

The most studied CACDs are those synthesized from CA and urea, and the structure of low-molecular-weight fluorophores, forming *in situ*, are well-documented.[8,15,22] Hence, citrazinic acid (CZA) and 4-hydroxy-1*H*-pyrrolo[3,4-*c*]pyridine-1,3,6(2*H*,5*H*)-trione (HPPT) were selected as model systems because their molecular structures contain both basic and acidic protic groups, that let us envision the existence of diverse tautomers, together with ionized forms depending on the pH environment. This makes them ideal candidates for investigating how these factors (tautomerism and pH) influence PL properties.

Additionally, CAGly was included in our study as its molecular structure comprises the DPR moiety and it has been classified as a DPR-type MF, showing weak QY and excitation dependent fluorescence.[8]

Neutral and charged CZA and HPPT tautomers have been considered in previous computational investigations.[14,41–44] These studies, however, have not been carried out exhaustively as to the best of our knowledge the CZA keto tautomer has not been previously claimed as the most stable tautomer, as we will demonstrate later in this work. In addition, the CZA keto tautomer comes up by following the formation mechanism (Scheme 1).

We started our investigation by searching for all tautomers of neutral CZA, HPPT and CAGly by using CREST (see Methods sections for further details). From these results, the keto-tautomer of CZA shows up as the most stable, later confirmed at a quantum chemistry level. CREST was also employed to locate the most probable tautomers of the ionized forms of the three evaluated MFs: those resulting from removing one, two or three protons (when possible) as simulating an increase of pH or those resulting from protonation as simulating extreme acidic conditions where neutral forms may be protonated to some extent.[17] Optimization with DFT and TD-DFT of selected tautomers (those obtained with CREST within an energy window of 20 kcal mol^{-1}) at both S_0 and S_1 states, respectively, let us establish the tautomeric ratios for the different pH-dependent forms.

Predominant tautomeric forms

According to Gibbs energy differences, we account for Boltzmann equilibrium populations of individual tautomers (see Methods section), in both S_0 and S_1 states. Schemes 2–4, collect those neutral and ionized tautomers, featuring populations different from zero of CZA, CAGly and HPPT, respectively.

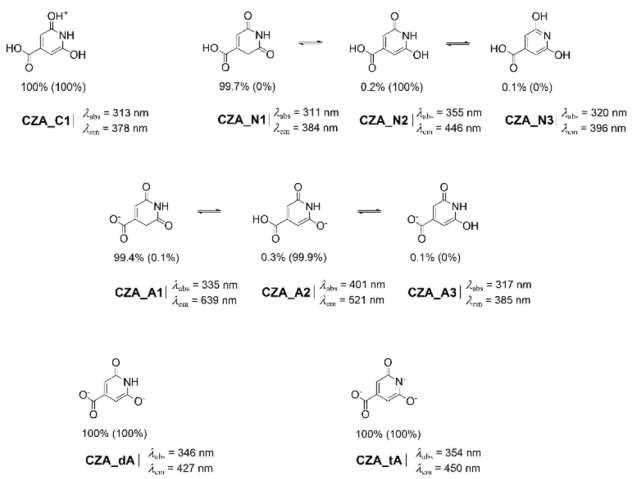

Scheme 2 Tautomeric forms of CZA with non-zero populations which may coexist in the dynamical acid–base equilibrium: **C** (cation); **N** (neutral); **A** (anion); **dA** (dianion); **tA** (trianion). Relative populations in S_0 (those in S_1 shown in brackets).

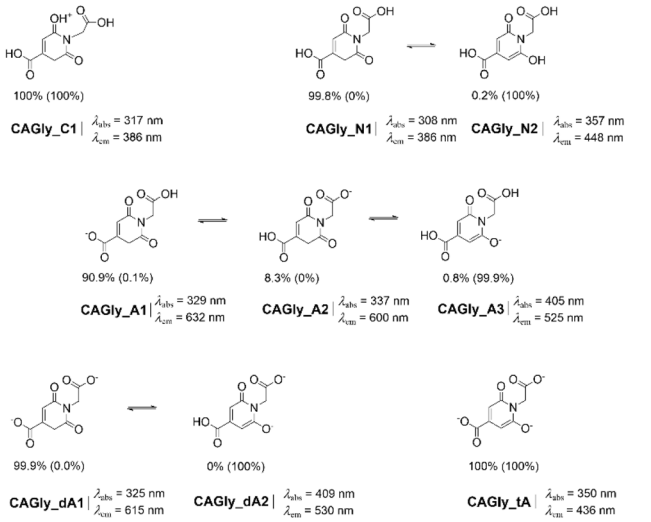

Scheme 3 Tautomeric forms of CAGly with non-zero populations in S_0 or/and S_1 states that may coexist in the dynamical acid–base equilibrium: **C** (cation); **N** (neutral); **A** (anion); **dA** (dianion); **tA** (trianion). Relative populations in S_0 (those in S_1 shown in brackets).

Corresponding Gibbs energy of the ground and the first single excited states can be found in Tables S1–S3.

As far as neutral CZA, our results (Scheme 2) reveal the almost exclusive predominance of the keto-tautomer, with a keto (**CZA_N1**)–enol (**CZA_N2**) ratio of *ca.* 99.7/0.2 (ΔG = +3.8 kcal mol^{-1}), in S_0 state, with a contribution of 0.1% of **CZA_N3** (ΔG = +4.1 kcal mol^{-1}).[45] To assess whether micro-solvation could influence the relative stability of the tautomers, we performed additional calculations including up to seven explicit water molecules in representative microsolvated clusters. In all cases, microsolvation preserved the preference for the keto tautomer (), which remained more stable than **CZA_N2** or **CZA_N3** (Fig. S1). These results indicate that specific hydrogen-bonding interactions do not overturn the stability trend predicted with the implicit solvation model. Furthermore, the **CZA_N1** → **CZA_N2** tautomerization pathway was characterized, yielding a transition-state barrier of 17.2 kcal mol^{-1},

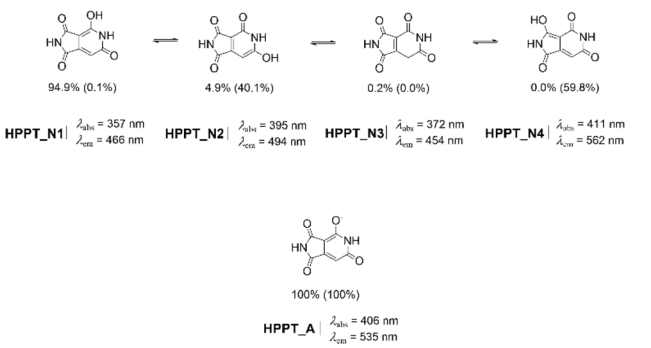

Scheme 4 Tautomeric forms of HPPT with non-zero populations that may coexist (see text) in the dynamical acid–base equilibrium: **N** (neutral) and **A** (anion). Relative populations in S_0 (those in S_1 shown in brackets).

confirming that the interconversion is limited by both thermodynamic and kinetic factors. Overall, these analyses demonstrate that even when explicit microsolvation is considered, the population of the enol tautomer is expected to remain low under the studied conditions.

We recall that the keto form, **CZA_N1**, featuring the DPR moiety, is the structure obtained following the mechanistic path described in Scheme 1, while the **CZA_N2** or **CZA_N3** are both the commonly ones used to depict it. To substantiate our computational results, we conducted a literature search,[27,41,44] to collect NMR data reported for CZA. Nevertheless, NMR spectra of CZA have been acquired either in D_2O–NaOD or DMSO-d_6, conditions under which strong solvent effects (double deprotonation or specific intermolecular hydrogen bond,[46,47] IHB) significantly alter the tautomeric equilibrium. Consequently, these data cannot be directly compared to the neutral keto tautomer (**CZA_N1**). Nevertheless, the comparative analysis in DMSO-d_6 is consistent with the presence of **CZA_N1**, though **CZA_N2** and **CZA_N3** may be majority as both can established up to three IHB's with DMSO. To address this point, we performed a full computational analysis including explicit-solvent DFT models and simulated NMR spectra, which are discussed in detail in the SI.

A similar keto–enol tautomeric ratio ($N_{\mathbf{N1}}/N_{\mathbf{N2}} = 99.8/0.2$) is obtained for neutral CAGly (Scheme 3). It is worth mentioning that the keto tautomer, **CAGly_N1**, is indeed the structure used to represent it.[8] To further support this assignment, we conducted a computational analysis to compare the calculated chemical shifts with the DMSO-d_6 NMR experimental data reported in ref. 8. The results are consistent with the proposed structure, suggesting that the experimental spectra can be explained by a mixture of **CAGly_N1** and **CAGly_N2** whose relative abundances are influenced by IHBs with DMSO, as also observed for CZA.

Interestingly, the tautomeric ratio is reversed in the S_1 state, where the enol tautomer becomes the only species with a non-zero population for both CZA (**CZA_N2***) and CAGly (**CAGly_N2***). In the excited state, the enol form is favored by a Gibbs energy difference of approximately 10 kcal mol^{-1}, leading to its exclusive population at the S_1 state.

When analyzing the anionic species, we found a similar behavior: although the most stable anion in the S_0 state corresponds to the keto tautomer, this preference no longer holds in the S_1 state.

Four anionic structures were identified for CZA (see SI), although only three of them are significantly representative of the tautomeric distribution in the ground state (Scheme 2). The most stable anion, **CZA_A1**, which retains the DPR moiety, lies 3.2 kcal mol^{-1} below the enol-like tautomer **CZA_A2**. In contrast, and in close analogy to the behavior observed for the neutral species, **CZA_A2** becomes the most stable form in the S_1 state, accounting for 99.9% of the excited-state population. The keto-type anion **CZA_A1*** is disfavored in S_1 (ΔG = 4.2 kcal mol^{-1}) and contributes only a negligible 0.1% to the population.

A similar situation is observed for the anionic species (**A**) of CAGly. Because CAGly contains two carboxylic groups, first deprotonation occurs preferentially at the most acidic one—derived from the citric acid fragment (Scheme 1)—leading to **CAGly_A1** as the most stable anion. The tautomer **CAGly_A2** lies close in energy ($\Delta G = 1.4$ kcal mol^{-1}), while **CAGly_A3** is higher in energy ($\Delta G = +2.8$ kcal mol^{-1}). These relative stabilities result in ground-state (S_0) populations of 90.9%, 8.3%, and 0.8% for **CAGly_A1**, **CAGly_A2**, and **CAGly_A3**, respectively. In the S_1 state, however, the situation reverses: **CAGly_A3*** becomes by far the most stable anion and thus the dominant phototautomer, with **CAGly_A1*** contributing only marginally (ΔG = +4.1 kcal mol^{-1}).

Upon second and third deprotonation of CZA, only the enol-like tautomers—**CZA_dA** and **CZA_tA**, respectively—which possess the 2-pyridone moiety, retain a non-zero population in both the S_0 and S_1 states. This behavior contrasts with that of CAGly, where the dianion **CAGly_dA** still features the DPR moiety and remains the most stable species in S_0, while the enol form becomes overwhelmingly favored in the S_1 state, reaching a population of 99.7%. Upon third deprotonation, CAGly yields **CAGly_tA**, which adopts an enol-like structure and is the sole species present in both S_0 and S_1.

Concerning HPPT, it has two fused rings and a larger number of carbonyl and amino groups, increasing the number of possible tautomers (Scheme 4), making different its PL properties: the keto/enol tautomerization is not playing any role but more than one phototautomer can coexist in the ground or in the excited state.

The most stable neutral tautomer of HPPT is **HPPT_N1** (94.9%) at S_0 which features the most common molecular representation, and it agrees with other findings,[29] yet we found **HPPT_N2** with non-zero probability ($N_{\mathbf{N2}} = 4.9\%$). Notably, **HPPT_N2*** reaches a population of 40.1% at S_1 and would be coexisting with **HPPT_N4*** ($N_{\mathbf{N4*}} = 59.8\%$), being the population of **HPPT_N1*** close to zero. It is also noted that **HPPT_N3**, the keto tautomer, has almost negligible population at both S_0 and S_1 states.

Despite the larger number of carbonyl and amino groups, tautomers of the anionic form limits to one, **HPPT_A1**. Two tautomers for the dianionic form were located, **HPPT_dA1** and **HPPT_dA2**, but the latter with only a minor contribution at S_1 state ($N_{\mathbf{dA2*}} = 1.7\%$). Similarly, the cationic form in the ground state is limited to one tautomer, **HPPT_C1**, but it vanishes at S_1, being replaced by two tautomers **HPPT_C2** and **HPPT_C3**, with populations of $N_{\mathbf{C2*}} = 98.6\%$ and $N_{\mathbf{C3*}} = 1.4\%$, respectively. However, HPPT has been described as a superacid[29] therefore, cationic species are predicted to be present only under extremely acidic conditions. In addition, it has been found that hydrolysis of **HPPT_A1** occurs before deprotonation, leading to a non-emissive compound.[29] Nevertheless, we have included these forms in the SI for completeness.

PL pathways

For those tautomers with populations different from zero in the S_0 or S_1 states, we have computed the largest absorption wavelength, and the emission wavelength from the optimized first single excited state. These values are collected in Schemes 2–4.

As noted above, the most stable tautomer in the ground state does not necessarily remain so in the excited state and more worthy, it may turn out that it is neither the phototautomer. This is the case for both CZA and CAGly. Our results indicate that the absorption maxima of **CZA_N1** and **CAGly_N1** are located at 311.1 nm and 308.2 nm, respectively, but emission from S_1 occurs within the UV spectrum region. In contrast, the excited-state tautomers **CZA_N2*** and **CAGly_N2***, which are the sole tautomeric species present in the S_1 state, shows fluorescence at 443 nm and 448 nm, respectively, in good agreement with previously reported experimental data.[8,27] These findings lead us to consider an excited state tautomerization before emission could happen; a process usually claimed to explain PL, specifically, when large Stokes shifts are observed.[48] Accordingly, photoexcitation converts the neutral CZA tautomer **CZA_N1** into **CZA_N1***, which subsequently undergoes keto to enol tautomerization leading to **CZA_N2***. This transformation is strongly thermodynamically favored ($\Delta G_{\mathbf{N1^*\rightarrow N2^*}} = -24.0$ kcal mol^{-1}) and is associated with a low kinetic barrier ($TS_{\mathbf{N1^*\rightarrow N2^*}} = 2.9$ kcal mol^{-1}) making it fully accessible. The resulting **CZA_N2*** is then responsible for the observed fluorescence emission (Fig. 1). Looking at the molecular orbitals involved in the **N1** → **N1*** electronic transition (Fig. 1), it corresponds to a weak n → π* excitation[27] ($f \approx 0$; as expected in symmetry-forbidden electronic transitions)[49] originating from the C=O lone pair while **N2** ← **N2*** results from a more intense transition of π ← π* character ($f = 0.12$).

Cationic species of CZA and CAGly may become predominant over their neutral counterparts under sufficiently acidic conditions (pH < 1).[22,27] Only one cationic tautomer (Schemes 2 and 3) may exist with population different from zero but with emission in the UV region. When the pH is increased, the equilibrium progressively shifts toward the deprotonated species, becoming noticeable above pH ≈ 4 according to our pK_a estimations (see SI). As commented above, the most stable anion for CZA and CAGly in the ground state no longer holds in the S_1 state yet, upon photoexcitation **CZA_A1*** and **CAGly_A1*** may eventually experience ESIPT leading, respectively, to the corresponding phototautomer **CZA_A2*** and **CAGly_A3*** with fluorescence emission at 521 nm ($f = 0.17$) and 525 nm ($f = 0.16$), respectively. Upon further deprotonation, CZA and CAGly yield **CZA_dA** (pH > 11) and **CAGly_dA1** (4 < pH < 7), respectively. In the case of CZA, both **CZA_dA** and the trianionic **CZA_tA** are predicted to be the most stable tautomers in both the ground (S_0) and excited (S_1) states. These species display fluorescence emissions at 433 nm ($f = 0.25$) and 450 nm ($f = 0.18$). For dianionic CAGly, an ESIPT pathway must be considered—consistent with the behavior observed for the other protonation states—from **CAGly_dA1*** ($\lambda_{em} = 615, f \approx 0$) to **CAGly_dA2*** ($\lambda_{em} = 530$ nm, $f = 0.15$) to rationalize the presence of intense fluorescence.

Regarding the optical properties of HPPT, previously reported experimental data[29] show absorption maxima at approximately 365 nm and 405 nm, corresponding to the neutral and anionic forms, respectively, which agree well with the computed values for **HPPT_N1** ($N_{\mathbf{N1}} = 96.4\%$; $\lambda_{abs} = 357$ nm; $f = 0.18$) and **HPPT_A** ($N_{\mathbf{A}} = 100\%$; $\lambda_{abs} = 406$ nm; $f = 0.18$), respectively (Scheme 4). Our computational results indicate that diverse radiative pathways may occur after photoexcitation of neutral **HTTP_N1** at 357 nm yielding **HPPT_N1*** (Fig. 2). These include: (i) ESIPT leading to the two stable tautomers in the S_1 state, **HPPT_N2*** and **HPPT_N4***; both readily accessible in protic solvents. Their population-weighted emission maximum is predicted near 536 nm (Fig. S8), although ESIPT may preferentially produce the most stable tautomer, **HPPT_N4***, which emits at $\lambda_{em} = 562$ nm, in line with literature experimental data;[14] and (ii) excited-state deprotonation (ESDP) of **HPPT_N1***, generating **HPPT_A***, which emits at 535 nm ($f = 0.19$). This emission is also obtained when **HPPT_A** is the sole species present in solution, in agreement with the experimentally recorded data (in the pH range 1–10).[29]

Keto–enol ESIPT transition state

ESIPT processes in fluorescent organic molecules are very common.[31–36] In many of them, the ground state molecular structure features an intramolecular hydrogen bond, IHB, leading to a stable six-membered ring containing the –N–H···O=C– or N–H···N=C– moieties. In these kinds of systems, it

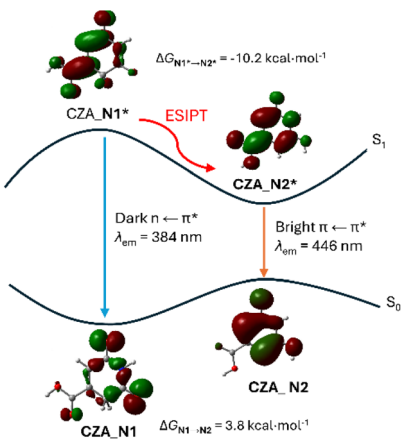

Fig. 1 ESIPT from keto (**CZA_N1***) to enol phototautomer (**CZA_N2***) explaining the PL of CZA (a similar process has found for neutral CAGly with similar values).

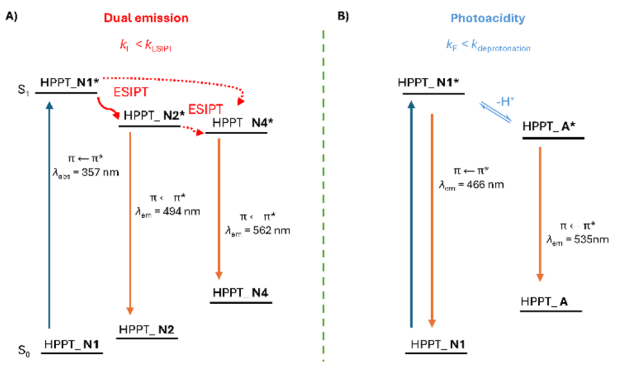

Fig. 2 Schematic representation of the radiative pathways accessible to **HPPT_N1**: (A) ESIPT to phototautomers **HPPT_N2*** and **HPPT_N4*** or (B) ESDP to **HPPT_A1*** phototautomer.

has been noted that polar protic solvents reduce ESIPT as solvent molecules could limit this incipient ESIPT transition state toward the enol tautomer –N···H–O/N–C–.[31,50,51]

This is not the case for CZA and CAGly systems, instead we claim water assisted keto → enol (pseudo)[48,50] ESIPT to rationalize the observed PL properties of CZA and CAGly as model systems for DPR MFs that may help to explain optical features of CACDs containing these MF's.

ESIPT may occur either reversibly or irreversibly and can operate under kinetic or thermodynamic control. Each regime exhibits characteristic photophysical features, as demonstrated in numerous experimental studies, although the interpretation of ESIPT signatures can be challenging due to the influence of multiple competing factors.[32]

Computational studies aimed at quantifying ESIPT energy barriers are still limited, and those available rely on constrained scans of the S_1 and S_0 potential-energy surfaces (PES) rather than on the explicit identification of transition states.[52,53] Therefore, no literature data exist for direct benchmarking of our computed ESIPT transition states and their associated barriers. Likewise, virtually no studies have examined water-assisted ESIPT in the excited state, despite the well-established role of water in lowering proton-transfer barriers in the ground state.[54] In agreement with these ground-state findings, our calculations show a substantial reduction in the keto-to-enol barrier when explicit water molecules are included (see above). This behavior provided a strong motivation for applying the same strategy in the excited state to locate the corresponding S_1 transition states.

We have located the transition state for the keto to enol tautomerization at S_1, for CZA. Notably, the activation energy significantly reduces on going from none up to three water molecules. We have confirmed this asynchronous TS[54] connects to the local minimum corresponding to the reactant (local minimum on the S_1 PES after some steps of relaxation from the initially excited Franck–Condon (F–C*) state[32,55]) from which the barrier is computed ($\Delta G_{3\ W\ \mathbf{CZA\_N1^*\rightarrow CZA\_N2^*}}^{\#} = 2.8$ kcal mol^{-1}, Fig. 3).[56] The thermodynamics is also favoured ($\Delta G = -24.0$ kcal mol^{-1} from local minima connected to the TS). This large energy difference suggests an irreversible regime governing the ESIPT process, leading to emission exclusively from **CZA_N2***.[32]

At pH values above 4, where the anionic species of CZA would be present—or even constitute the predominant form—ESIPT must occur for bright fluorescence to be observed (Table S1). Thus, we computed a slightly lower barrier for the **CZA_A1*** → **CZA_A2*** conversion ($\Delta G_{3\ W\ \mathbf{CZA\_A1^*\rightarrow CZA\_A2^*}}^{\#} = 2.2$ kcal mol^{-1}) than for neutral form (see above). However, the thermodynamic driving force is weaker ($\Delta G = -5.1$ kcal mol^{-1}), suggesting that the process may proceed in a reversible manner. In this scenario, thermodynamic rather than kinetic factors may determine the presence of the **CZA_A1*** form in the emission (Table S1). As **CZA_dA** and **CZA_tA** correspond to enol tautomers in the ground state, ESIPT is not needed to explain their ~427–450 nm emission (being emission at 446 nm from the **CZA_N2***). Overall, CZA will feature near pH independent emission spectrum. This could be experimentally seen as having no pH effects on the emission wavelength.[29,30]

An analogous analysis with CAGly lead us to find a low barrier for **CAGly_N1*** to **CAGly_N2*** tautomerization at 2.5 kcal mol^{-1} and favourable thermodynamics $\Delta G = -21.6$ kcal mol^{-1}. For the anion form a similar outcome as with CZA is expected. However, as CAGly anion, dianion and neutral form may coexist in neutral pH (see SI), more complex emission spectrum may be expected.[8]

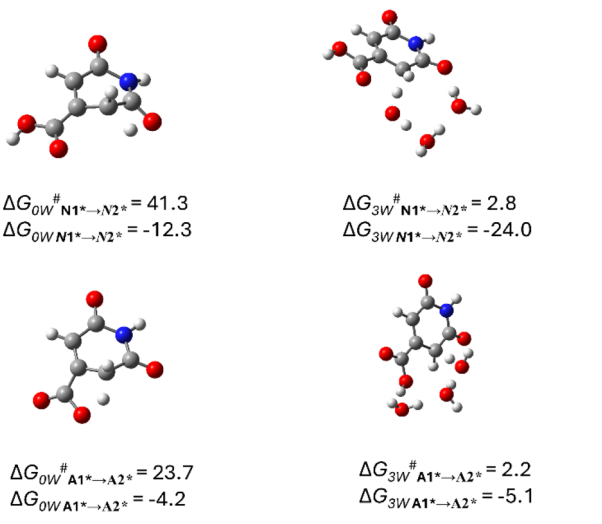

Fig. 3 ESIPT transition state structures together with the corresponding Gibbs energy barrier and keto–enol Gibbs energy differences ($\Delta G^{\#}$ and ΔG, respectively, in kcal mol^{-1}) when assisted by either three water molecules (3 W) or none (0 W), for neutral CZA and anionic CZA. Equivalent structures and energies are obtained for CAGly.

Conclusions

Based on CREST screening and DFT/TD-DFT refinement calculations, our results reveal that the keto tautomer (DPR moiety) predominates in the ground state (S_0) for CZA and CAGly, whereas the enol tautomer (recovering the 2-pyridone moiety) becomes the main phototautomer in the excited state (S_1) through ESIPT, well reproducing the literature experimental data. Additionally, we found that water molecules assist in lowering the ESIPT barrier, underscoring the importance of solvent effects. This behaviour is expected to have implications in PL when these MFs are dissolved in solvents other than water. Further, our computational study indicates that multiple radiative pathways may operate following photoexcitation of the most stable neutral HTTP tautomer, potentially leading to emission at a wavelength consistent with that expected for the anionic HPPT form.

Our results evidence that understanding tautomeric dynamics and their pH dependence provides a molecular-level basis for tuning the optical properties of CACDs. This study substantiates that tautomerism and pH are key factors determining PL properties of CA-derived MFs, which may also serve as models for understanding CA-based biomaterials optical behaviour.

Although additional experimental data would certainly strengthen the present conclusions, computational chemistry can still provide valuable insight into photophysical processes that remain only partially explored—particularly the detailed ESIPT mechanisms in these MFs. Future work should therefore integrate quantum molecular dynamics (QMD) simulations to better capture the role of the solvent, including the conditions under which dimers or higher aggregates may form and whether the most stable dimer in the ground state remains preferred in the S_1 state. Moreover, classical or hybrid MD simulations could help describe the interactions among the different tautomeric and ionic forms in the presence of model carbon dots, thereby establishing a more complete picture of how these species behave in realistic environments. Such studies would significantly advance our understanding of the photophysics of these MFs and of the CDs derived from them.

Methods

We selected CZA, CAGly and HPPT MFs as case study model systems to explore the effect of tautomerism and pH on PL properties.

Prototropic chemical space within the acid–base equilibria

CZA, CAGly and HPPT were submitted to protonation/deprotonation sites and tautomerism screenings using the GFN2-xTB level as implemented in CREST program[57] to locate the most probable tautomers at different pH values, from high acidic (tautomers of the cationic forms) to slightly acidic (tautomers of neutral forms), to high basic environments (tautomers of the anionic, dianionic or trianionic forms – when possible). It is worth mentioning that protonated and deprotonated species were obtained by adding or removing protons at chemically plausible acidic/basic sites. Although this does not model pH explicitly, these ionic forms correspond to the species that would predominate under sufficiently acidic or alkaline conditions. From CREST (GFN-xTB) generated tautomer ensemble within the default energy window of 20 kcal mol^{-1}, all distinct tautomeric and conformational minima were identified, and only those structures corresponding to chemically meaningful interconverting forms were retained for refinement. Each unique tautomeric form and each relevant low-energy conformer associated with that tautomer was re-optimized at the DFT and TD-DFT levels. This protocol has been successfully employed previously.[58]

Population and PL properties

The ground state (S_0) and the first singlet excited state (S_1) optimized geometries and corresponding Gibbs energies of selected tautomer derived from CREST were obtained, respectively, by means of DFT and TD-DFT (within the linear response (LR) approximation to obtain absorption wavelengths and the state specific (SS) for the emission wavelength from S_1), as implemented in Gaussian 16.[59] Frequency calculations were undertaken to confirm the nature of each stationary point, yielding one imaginary frequency for a transition state (TS), corresponding to the expected process, and all positive frequencies for a minimum. The connectivity of the TS and their adjacent minimum was confirmed by intrinsic reaction coordinate (IRC) calculations. The B3LYP hybrid functional along with the 6-311++G(2d,2p) basis set was the method of choice.[18,60] Solvent (water) effects were included in all calculations by means of the solvation model based on density (SMD).[61] Boltzmann equilibrium populations[62] at 298 K, N (in %), were obtained by using eqn (1), where G_i is the Gibbs energy of the tautomer whose population is being calculated, and G_j refers to the Gibbs energies of the remaining tautomers.

$$N_i = \frac{\exp\left(-\frac{G_i}{RT}\right)}{\sum_j \exp\left(-\frac{G_j}{RT}\right)} \times 100 \quad (1)$$

When applying the Boltzmann distribution to obtain relative tautomer populations in S_1 is assumed that vibrational relaxation and tautomer interconversion in the excited state occur much faster than the S_1 lifetime. This allows S_1 to reach a quasi-thermal equilibrium, so $\Delta G(S_1)$ reliably determines the population distribution.

Author contributions

L. E. conceptualized the work writing – review & editing, software, formal analysis, investigation, data curation, conceptualization. N. O. review & editing, software, formal analysis and data curation.

Conflicts of interest

The authors declare that they have no known competing financial interests or personal relationships that could have appeared to influence the work reported in this paper.

Data availability

The supporting data have been provided as part of the supplementary information (SI). Supplementary information is available. See DOI: https://doi.org/10.1039/d6ra00206d.

Acknowledgements

Authors thank Xunta de Galicia for financial support through GRC-ED431C 2024/21. Funding for open access charge: Universidade de Vigo/CISUG.

Notes and references

1 D. Ozyurt, M. Al Kobaisi, R. K. Hocking and B. Fox, Properties, synthesis, and applications of carbon dots: A review, *Carbon Trends*, 2023, **12**, 100276.
2 S. N. Baker and G. A. Baker, Luminescent carbon nanodots: emergent nanolights, *Angew. Chem., Int. Ed.*, 2010, **49**, 6726.

3 J. Shen, Y. Zhu, X. Yang and C. Li, Graphene quantum dots: emergent nanolights for bioimaging, sensors, catalysis and photovoltaic devices, *Chem. Commun.*, 2012, **48**, 3686.
4 K. Wang, Z. Gao, G. Gao, Y. Wo, Y. Wang, G. Shen and D. Cui, Systematic safety evaluation on photoluminescent carbon dots, *Nanoscale Res. Lett.*, 2013, **8**, 122.
5 L. Vallan and H. Imahori, Citric Acid-Based Carbon Dots and Their Application in Energy Conversion, *ACS Appl. Electron. Mater.*, 2022, **4**, 4231.
6 C. Hu, M. Li, J. Qiu and Y.-P. Sun, Design and fabrication of carbon dots for energy conversion and storage, *Chem. Soc. Rev.*, 2019, **48**, 2315.
7 C. L. Shen, Q. Lou, J. H. Zang, K. K. Liu, S. N. Qu, L. Dong and C. X. Shan, Near-Infrared Chemiluminescent Carbon Nanodots and Their Application in Reactive Oxygen Species Bioimaging, *Adv. Sci.*, 2020, **7**, 1903525.
8 X. Zhiwei, J. P. Kim, Q. Cai, Y. Zhang, J. Guo, R. S. Dhami, L. Li, B. Kong, Y. Su, K. A. Schug and J. Yang, Synthesis and characterization of citrate-based fluorescent small molecules and biodegradable polymers, *Acta Biomater.*, 2017, **50**, 361.
9 W. Kasprzyk, S. Bednarz, P. Żmudzki, M. Galica and D. Bogdał, Novel efficient fluorophores synthesized from citric acid, *RSC Adv.*, 2015, **5**, 34795.
10 S. Mura, L. Stagi, R. Ludmerczki, L. Malfatti and P. Innocenzi, Reversible Aggregation of Molecular-Like Fluorophores Driven by Extreme pH in Carbon Dots, *Materials*, 2020, **13**, 3654.
11 J. Schneider, C. J. Reckmeier, Y. Xiong, M. von Seckendorff, A. S. Susha, P. Kasák and A. L. Rogach, Molecular Fluorescence in Citric Acid-Based Carbon Dots, *J. Phys. Chem. C*, 2017, **121**, 2014.
12 W. Kasprzyk, P. P. Romańczyk, K. Starzak, A. Wysocka, Ł. Waluda, T. Świergosz, N. V. Bashmakova, G. V. Klishevich, A. M. Dmytruk, I. S. Klyuyev and M. V. Bondar, Toward Better Understanding of Molecular Fluorophore Covalent Binding to Carbon Dots, *Small Struct.*, 2025, **6**, 2400583.
13 Y. Song, S. Zhu, S. Zhang, Y. Fu, L. Wang, X. Zhao and B. Yang, Investigation from chemical structure to photoluminescent mechanism: a type of carbon dots from the pyrolysis of citric acid and an amine, *J. Mater. Chem. C*, 2015, **3**, 5976.
14 W. Kasprzyk, T. Świergosz, P. P. Romańczyk, J. Feldmann and J. K. Stolarczyk, The role of molecular fluorophores in the photoluminescence of carbon dots derived from citric acid: current state-of-the-art and future perspectives, *Nanoscale*, 2022, **14**, 14368.
15 W. Kasprzyk, T. Świergosz, S. Bednarz, K. Walas, N. V. Bashmakova and D. Bogdał, Luminescence phenomena of carbon dots derived from citric acid and urea – a molecular insight, *Nanoscale*, 2018, **10**, 13889.
16 A. Matwijczuk, D. Karcz, R. Walkowiak, J. Furso, B. Gładyszewska, S. Wybraniec, A. Niewiadomy, G. P. Karwasz and M. Gagoś, Effect of Solvent Polarizability on the Keto/Enol Equilibrium of Selected Bioactive Molecules from the 1,3,4-Thiadiazole Group with a 2,4-Hydroxyphenyl Function, *J. Phys. Chem. A*, 2017, **121**, 1402.
17 M. Sitzmann, W.-D. Ihlenfeldt and M. C. Nicklaus, Tautomerism in large databases, *J. Comput. Aided Mol. Des.*, 2010, **24**, 521.
18 Y. C. Martin, Let's not forget tautomers, *J. Comput. Aided Mol. Des.*, 2009, **23**, 693.
19 L. Antonov, V. Deneva, S. Simeonov, V. Kurteva, D. Nedeltcheva and J. Wirz, Exploiting tautomerism for switching and signaling, *Angew. Chem., Int. Ed.*, 2009, **48**, 7875.
20 M. Sholokh, R. Improta, M. Mori, R. Sharma, C. Kenfack, D. Shin, K. Voltz, R. H. Stote, O. A. Zaporozhets, M. Botta, Y. Tor and Y. Mély, Tautomers of a Fluorescent G Surrogate and Their Distinct Photophysics Provide Additional Information Channels, *Angew. Chem., Int. Ed.*, 2016, **55**, 7974.
21 B. Gauthier-Manuel, C. Benmouhoub and B. Wacogne, Fluorescence Spectra of Prototropic Forms of Fluorescein and Some Derivatives and Their Potential Use for Calibration-Free pH Sensing, *Sensors*, 2024, **24**, 1705.
22 J. P. Kim, Z. Xie, M. Creer, Z. Liuc and J. Yang, Citrate-based fluorescent materials for low-cost chloride sensing in the diagnosis of cystic fibrosis, *Chem. Sci.*, 2017, **8**, 550.
23 L. Placer, L. Estévez, I. Lavilla, F. Pena-Pereira and C. Bendicho, Assessing citric acid-derived luminescent probes for pH and ammonia sensing: a comprehensive experimental and theoretical study, *Anal. Chim. Acta*, 2021, **1186**, 339125.
24 Y. Hu and A. Bianco, Unraveling the synthesis-structure-property relationship in aromatic amino acids-derived carbon dots, *Carbon*, 2025, **235**, 120073.
25 A. Sharma, T. Gadly, A. Gupta, A. Ballal, S. K. Ghosh and M. Kumbhakar, Origin of Excitation Dependent Fluorescence in Carbon Nanodots, *J. Phys. Chem. Lett.*, 2016, **7**, 3695.
26 A. Cappai, C. Melis, L. Stagi, P. C. Ricci, F. Mocci and C. M. Carbonaro, Insight into the Molecular Model in Carbon Dots through Experimental and Theoretical Analysis of Citrazinic Acid in Aqueous Solution, *J. Phys. Chem. C*, 2021, **125**, 4836.
27 L. Stagi, S. Mura, L. Malfatti, C. M. Carbonaro, P. C. Ricci, S. Porcu, F. Secci and P. Innocenzi, Anomalous Optical Properties of Citrazinic Acid under Extreme pH Conditions, *ACS Omega*, 2020, **5**, 10958.
28 W. J. Sell and T. H. Easterfield, LXXIII-Studies on Citrazinic Acid. Part I, *J. Chem. Soc. Trans.*, 1893, **63**, 1035.
29 W. Kasprzyk, P. P. Romańczyk, S. S. Kurek and T. Świergosz, A switchable green emitting dye and its phenomenal properties: implications for the photoluminescence features of carbon dots, *Nanoscale*, 2024, **16**, 17079.
30 S. K. Cushing, M. Li, F. Huang and N. Wu, Origin of Strong Excitation Wavelength Dependent Fluorescence of Graphene, *ACS Nano*, 2014, **8**, 1002.
31 S. K. Behera, S. Y. Park and J. Gierschner, Dual Emission: Classes, Mechanisms, and Conditions, *Angew. Chem., Int. Ed.*, 2021, **60**, 22624.

32 V. I. Tomina, A. P. Demchenkob and P.-T. Chouc, Thermodynamic vs. kinetic control of excited-state proton transfer reactions, *J. Photochem. Photobiol., C*, 2015, **22**, 1.

33 Z.-Y. Liu, Y.-C. Wei and P.-T. Chou, Correlation between Kinetics and Thermodynamics for Excited-State Intramolecular Proton Transfer Reactions, *J. Phys. Chem. A*, 2021, **125**, 6611.

34 Y. Wang, M. Hu, Q. Yue, F. Xiaoqing and Y. Zhao, Insights into ESIPT-induced multicolor fluorescence emission in 2-(20-hydroxy-50-bromo) phenylbenzimidazole: a spectroscopic and TDDFT study, *RSC Adv.*, 2024, **14**, 39759.

35 F. He, H.-B. Li, H. Xu, J. Bai, Y. Cheng, X. Meng, W. Zhang, X. Fang, Y. Xu and T. Ding, ESIPT fluorophores derived from 2,3-dichloro-5,6-dicyano-p-benzoquinone based carbon dots for dual emission and multiple anti-counterfeiting, *Phys. Chem. Chem. Phys.*, 2021, **23**, 388.

36 J. Bai, W. Zhu, F. He, Y. Cheng, X. Meng, H. Xu, Y. Xu, W. Zhang, X. Fang and H.-B. Li, Excited-state intramolecular proton-transfer-induced dual fluorescence emission in 2,3-dichloro-5,6-dicyano-1,4-benzoquinone and resorcinol-based carbon dots, *Opt. Mater.*, 2022, **123**, 111845.

37 J. C. del Valle and J. Catalán, Kasha's rule: a reappraisal, *Phys. Chem. Chem. Phys.*, 2019, **21**, 10061.

38 K. Veys and D. Escudero, Anti-Kasha Fluorescence in Molecular Entities: Central Role of Electron−Vibrational Coupling, *Acc. Chem. Res.*, 2022, **55**, 2698.

39 L. R. Sigmon, J. Catazaro, M. Abdel-Rahman, C. Smith, C. Prasse and D. H. Fairbrother, Interrogating the photoluminescent properties of carbon dots using quantitative 13C NMR combined with systematic photobleaching, *Carbon*, 2025, **232**, 119796.

40 A. Wysocka, Ł. Waluda, R. Konefał and W. Kasprzyk, Liquid chromatography methods as a solution to inaccuracies associated with purity assessment of citric acid-based carbon dots, *Microchem. J.*, 2024, **205**, 111240.

41 V. Strauss, H. Wang, S. Delacroix, M. Ledendecker and P. Wessig, Carbon nanodots revised: the thermal citric acid/urea reaction, *Chem. Sci.*, 2020, **11**, 8256.

42 F. Mocci, C. Olla, A. Cappai, R. Corpino, P. C. Ricci, D. Chiriu, M. Salis and C. M. Carbonaro, Formation of Citrazinic Acid Ions and Their Contribution to Optical and Magnetic Features of Carbon Nanodots: A Combined Experimental and Computational Approach, *Materials*, 2021, **14**, 770.

43 S. Mura, L. Stagi, L. Malfatti, C. M. Carbonaro, R. Ludmerczki and P. Innocenzi, Modulating the Optical Properties of Citrazinic Acid through the Monomer-to-Dimer Transformation, *J. Phys. Chem. A*, 2020, **124**, 197.

44 X. Yao, Y. Wang, F. Li, J. J. Dalluge, G. Orr, R. Hernandez, Q. Cui and C. L. Haynes, Unconventional aliphatic fluorophores discovered as the luminescence origin in citric acid-urea carbon dots, *Nanoscale*, 2022, **14**, 9516.

45 We call attention's reader that in ref. 27 authors named keto and imine tautomers of CZA to what we have labelled as the enol **N2** and "imine" **N3**, respectively.

46 R. J. Abraham and M. Mobli, An NMR, IR and theoretical investigation of (1)H chemical shifts and hydrogen bonding in phenols, *Magn. Reson. Chem.*, 2007, **45**, 865.

47 P. G. Takis, K. D. Papavasileiou, L. D. Peristeras, G. C. Boulougouris, V. S. Melissas and A. N. Troganis, Unscrambling micro-solvation of–COOH and–NH groups in neat dimethyl sulfoxide: insights from 1H-NMR spectroscopy and computational studies, *Phys. Chem. Chem. Phys.*, 2017, **19**, 13710.

48 H. C. Joshi and L. Antonov, Excited-State Intramolecular Proton Transfer: A Short Introductory Review, *Molecules*, 2021, **26**, 1475.

49 D. Escudero, A. D. Laurent and D. Jacquemin, Time-Dependent Density Functional Theory: A Tool to Explore Excited States, in *Handbook of Computational Chemistry*, ed. J. Leszczynski, Springer, Dordrecht, 2015.

50 J. Konijnenberg, G. B. Ekelmans, A. H. Huizer and C. A. G. Varma, Mechanism and Solvent Dependence of the Solvent-catalysed Pseudo-intramolecular Proton Transfer of 7-Hydroxyquinoline in the First Electronically Excited Singlet State and in the Ground State of its Tautomer, *J. Chem. Soc., Faraday Trans. 2*, 1989, **85**, 39.

51 M. Tao, Y. Li, Q. Huang, H. Zhao, J. Lan, Y. Wan, Z. Kuang and A. Xia, Correlation between Excited-State Intramolecular Proton Transfer and Electron Population on Proton Donor/Acceptor in 2-(2′-Hydroxyphenyl)oxazole Derivatives, *J. Phys. Chem. Lett.*, 2022, **13**, 4486.

52 A. Watwiangkhama, T. Roongcharoena and N. Kungwan, Effect of nitrogen substitution and π-conjugation on photophysical properties and excited state intramolecular proton transfer reactions of methyl salicylate derivatives: theoretical investigation, *J. Photochem. Photobiol., A*, 2020, **389**, 112267.

53 S. Santra and N. Guchhait, Single vs dual steps enol-keto photoisomerisation: molecule with two ways symmetrical cyclic six-membered H-bonded network, *J. Photochem. Photobiol., A*, 2026, **476**, 117106.

54 W. P. Oziminski, The kinetics of water-assisted tautomeric 1,2-proton transfer in azoles: a computational approach, *Struct. Chem.*, 2016, **27**, 1845.

55 J. Zhao, H. Dong and Y. Zheng, Theoretical Insights Into the Excited State Double Proton Transfer Mechanism of Deep Red Pigment Alkannin, *J. Phys. Chem. A*, 2018, **122**, 1200.

56 The local minimum reactant is a worth noting that the computed barrier from the absolute minimum **CZA_N1***_3 W reaches 13.6 kcal mol¯1; a value incompatible with a sufficiently fast process to compete with fluorescence emission.

57 P. Pracht, S. Grimme, C. Bannwarth, F. Bohle, S. Ehlert, G. Feldmann, J. Gorges, M. Müller, T. Neudecker, C. Plett, S. Spicher, P. Steinbach, P. A. Wesołowski and F. Zeller, CREST—a program for the exploration of low-energy molecular chemical space, *J. Chem. Phys.*, 2024, **160**, 114110.

58 T. K. Harvey, K. Pota, M. M. Mekhail, D. M. Freire, D. A. Agbaglo, B. G. Janesko and K. N. Green, Predicting pK_a of flexible polybasic tetra-aza macrocycles, *RSC Adv.*, 2025, **15**, 10663.

59 M. J. Frisch, G. W. Trucks, H. B. Schlegel, G. E. Scuseria, M. A. Robb, J. R. Cheeseman, G. Scalmani, V. Barone, G. A. Petersson, H. Nakatsuji, X. Li, M. Caricato, A. V. Marenich, J. Bloino, B. G. Janesko, R. Gomperts, B. Mennucci, H. P. Hratchian, J. V. Ortiz, A. F. Izmaylov, J. L. Sonnenberg, D. Williams-Young, F. Ding, F. Lipparini, F. Egidi, J. Goings, B. Peng, A. Petrone, T. Henderson, D. Ranasinghe, V. G. Zakrzewski, J. Gao, N. Rega, G. Zheng, W. Liang, M. Hada, M. Ehara, K. Toyota, R. Fukuda, J. Hasegawa, M. Ishida, T. Nakajima, Y. Honda, O. Kitao, H. Nakai, T. Vreven, K. Throssell, J. A. Montgomery Jr, J. E. Peralta, F. Ogliaro, M. J. Bearpark, J. J. Heyd, E. N. Brothers, K. N. Kudin, V. N. Staroverov, T. A. Keith, R. Kobayashi, J. Normand, K. Raghavachari, A. P. Rendell, J. C. Burant, S. S. Iyengar, J. Tomasi, M. Cossi, J. M. Millam, M. Klene, C. Adamo, R. Cammi, J. W. Ochterski, R. L. Martin, K. Morokuma, O. Farkas, J. B. Foresman and D. J. Fox, *Gaussian 16, Revision C.01*, Gaussian, Inc, Wallingford CT, 2019.

60 Ç. Karaca, F. Bardak, E. Köse and A. Ataç, Experimental and computational insights into the electronic structures and absorption-emission characteristics of coumarin, C-6H, C-153, and C-343 dyes, *Spectrochim. Acta, Part A*, 2025, **335**, 125995.

61 A. V. Marenich, C. J. Cramer and D. G. Truhlar, Universal solvation model based on solute electron density and on a continuum model of the solvent defined by the bulk dielectric constant and atomic surface tensions, *J. Phys. Chem. B*, 2009, **113**, 6378.

62 D. A. M. Quarrie, *Statistical Mechanics*, University Science Books, Sausalito, 2000.